Journal of Polymer Research (2023) 30:8
https://doi.org/10.1007/s10965-022-03390-y

REVIEW PAPER

Synergetic photodegradation via inorganic–organic hybridization strategies: a review on preparations and applications of nanoparticle-hybridized polyaniline photocatalysts

Ying Fan[1] · Zhengkun Bai[1] · Qingmei Ge[1] · Nan Jiang[1] · Mao Liu[1] · Hang Cong[1] · Yunqian Zhang[2]

Received: 10 August 2022 / Accepted: 23 November 2022 / Published online: 2 December 2022

Abstract
Conjugated polymers such as polyaniline (PANI), polypyrrole, and polythiophene have attracted much attention owing to their good electrical conductivity, stability, ease of preparation, and high application potential. Among these conjugated polymers, PANI has attracted much attention in the field of photocatalysis owing to its ability to absorb visible light and rapidly separate the photoexcited electron–hole pairs. Recently, a large number of studies have shown that PANI can substantially increase the photocatalytic activity under both UV light and natural sunlight irradiation. Considering this most unique performance of PANI-based photocatalysis, the applications of PANI in the preparation of composite photocatalysts for the photocatalytic degradation of dyes, pharmaceuticals, and pesticides are summarized. In this review, the preparation methods, morphology, and photocatalytic properties of various composites are systematically studied. Synergistic effects between PANI and semiconductor nanomaterials or other carbon materials were found in many composite photocatalysts. Moreover, the mechanism of photocatalytic activity enhancement can be explained by analyzing the band structure of composite photocatalyst.

Keywords Polyaniline · Photodegradation · Composite photocatalyst · Organic pollutants

Introduction

In recent decades, the extensive use of organic dyes, antibiotics, pesticides, and other organic pollutants has caused large-scale environmental pollution [1–5]. To reduce water pollution, these pollutants are removed from wastewater using various technologies including biodegradation, adsorption, ozonation, photocatalytic degradation, physicochemical treatment, catalytic reduction, and coagulation/flocculation [6]. Recently, advanced oxidation processes (AOPs) have attracted much attention for the oxidation treatment of organic pollutants. In different AOPs, multiphase photocatalysis is one of the green chemical methods for the removal of various pollutants with low cost, wide application, and eco-friendly characteristic [7]. Electrons can be excited and transitioned from the valence band (VB) to the conduction band (CB), with irradiation at a certain wavelength on the surface of photocatalytic materials, leaving holes in the VB whose energy is equivalent to the band gap energy of the irradiated light [8]. The electrons and holes oxidize and reduce organic pollutants and mineralize these organic compounds into carbon dioxide, water, and inorganic acids [9]. Photocatalytic degradation of organic compounds using semiconductor materials such as TiO_2, ZnO, SnO_2, WO_3, ZrO_2, V_2O_5, CdS, CuO and MoO_3 has been reported [10–18]. In addition, semiconductor photocatalysts can also be used in photocatalytic hydrogen production and antimicrobial applications [19–21]. Although these traditional semiconductor photocatalysts have the advantages of high efficiency, convenient preparation, high stability, reusability, and environmental friendliness, they have also numerous disadvantages as follows: (i) The surface of metal oxides

✉ Hang Cong
hcong@gzu.edu.cn

✉ Yunqian Zhang
sci.yqzhang@gzu.edu.cn

[1] Enterprise Technology Center of Guizhou Province, Guizhou University, Guiyang 550025, China

[2] Key Laboratory of Macrocyclic and Supramolecular Chemistry of Guizhou Province, Guizhou University, Guiyang 550025, China

can only absorb less than 5% of visible and UV radiation for the wide bandgap, resulting in a quick recombination of the photoinduced electron–hole pairs and the limited ability to degrade organic pollutants [22]; (ii) organic pollutants can be completely degraded in the presence of semiconductor photocatalysts, but the formation of a large number of unwanted end products and intermediates is unavoidable in the oxidation of azo dyes [7]; (iii) agglomeration of metal oxide nanoparticles (NPs) decreases the surface area and active sites, reducing the photocatalytic performance and making it difficult to recover the catalyst [23]. To effectively solve the abovementioned problems and improve the photocatalytic activity, conductive materials have been used as electron acceptors to transfer photogenerated electrons, effectively blocking the recombination of photogenerated electron–hole pairs. Among many conductive materials, conductive polymers with excellent processability, including polyaniline (PANI), polypyrrole (PPy), and polythiophene (PT), have been widely studied in basic research and industrial applications [24]. PANI is one of the most attractive members of the intrinsically conductive polymer family because of facile preparation, unique doping mechanism, low toxicity, low cost, large surface area/volume ratio, excellent environmental stability, acid–base properties, and special redox properties [25]. For these reasons, PANI-based materials and composites have been used in numerous fields such as photovoltaics, anticorrosion, adsorption, biomedical equipment, sensors, electrochemistry, and electronics [26]. Particularly, PANI has a high absorption coefficient in the visible-light range and high mobility of charge carriers. In addition, PANI is an excellent electron donor and hole acceptor after irradiation [27]. Owing to these special properties, PANI has attracted much interest in photocatalysis. In this review, recent advanced compositions, preparation methods, testing conditions, possible mechanism, and improvement in photocatalytic efficiency of PANI-based composites are summarized.

Photocatalytic decomposition of dyes

Photocatalytic degradation of organic pollutants mainly involves dyes such as rhodamine B (RhB), methylene blue (MB), methyl orange (MO), malachite green (MG), Congo red (CR), and crystal violet. They have become the primary sources of water pollution, and their toxicity and carcinogenicity have attracted much attention [28–34]. Degradation of various dyes has been extensively studied in literature via the photocatalysis of pristine PANI or PANI-based composites [35–44].

Organic dyes can be divided in two basic groups [45]. Cationic dyes include a positive charge, usually localized on the nitrogen atom, which is balanced by a counter ion. MB, RhB, and safranin are important examples of cationic dyes and model pollutants in photodegradation. Anionic dyes usually carry a negative charge (sulfonic or carboxyl groups) and can be delivered as sodium salts. MO and CR are probably the most important members in this family, and they have been used as model substrates to evaluate the degradation reactivity of photocatalysts.

Degradation of MB using PANI composites

Rahman and Kar reported that the incorporation of PANI on TiO_2 efficiently degraded organic dye MB under UV-light exposure, and the proposed mechanism is shown in Fig. 1 [46]. Under UV-light irradiation, both PANI and

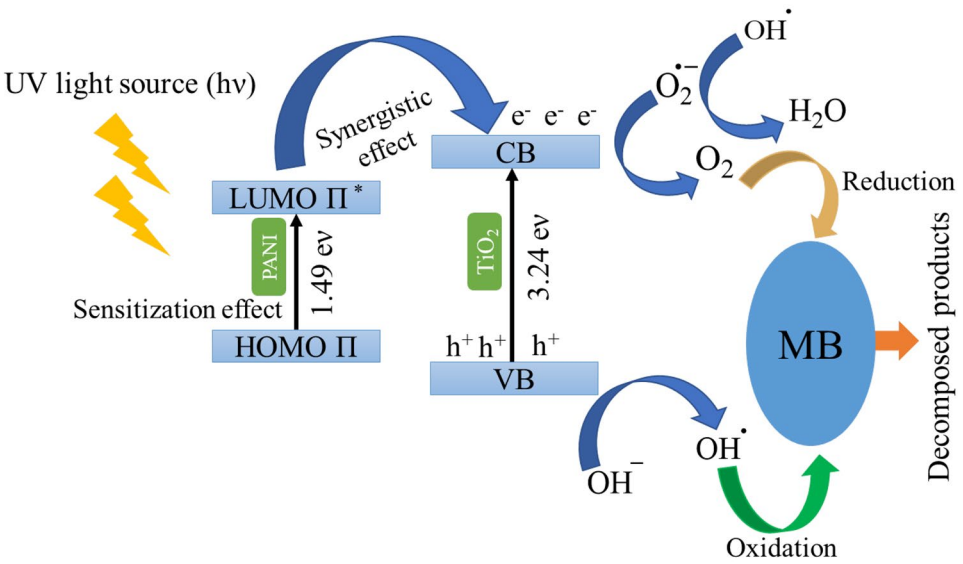

Fig. 1 Mechanism of PANI-TiO_2 photocatalytic dye degradation

TiO_2 generated electron–hole pairs with synergistic effect. The LUMO electrons in PANI were transferred to the CB of TiO_2, while the photogenerated holes in the VB of TiO_2 migrated to the HOMO of PANI. Moreover, the experimental results show that 0.6 M PANI-TiO_2 nanocomposite produced the highest dye degradation efficiency, with an improved efficiency of 2.5 times to pristine PANI and 3.1 times to TiO_2.

Novel PANI-$SrSnO_3$ (PANI/$SrSnO_3$) binary nanocomposites with different PANI contents (0 – 10 wt%) were successfully prepared using a simple and direct mechanical grinding process followed by an ultrasonic technique [47]. The XRD and FTIR studies exhibited the formation a standard single-phase of orthorhombic $SrSnO_3$ and the presence of PANI with perovskite $SrSnO_3$. All PANI/$SrSnO_3$ nanocomposites showed better photocatalytic efficiency on the degradation of MB dye than either free PANI or $SrSnO_3$ under UV irradiation. Particularly, 5% PANI/$SrSnO_3$ nanocomposite exhibited excellent catalytic performance with 83% destruction rate of MB within 4 h, which was nearly four folds of activity than free $SrSnO_3$ with sufficient stability and durability.

Besides combining with semiconductor nanomaterials to prepare composite photocatalysts, PANI can also be used to construct metal-free photocatalysts. Graphitic carbon nitride (g-C_3N_4) nanosheets (CNns) were modified by codoping PANI with an inorganic acid (hydrochloric acid, HCl) and an organic acid (phytic acid, PA) [48]. As a result of the synergistic effect of HCl and PA codoping on PANI through intrachain and interchain connection (Fig. 2), PANI/CNns obtained the characteristics of high electrical conductivity, large specific surface area, inhibition of charge recombination, and rich in free radicals, substantially improving the photocatalytic performance. When 1P1C sample (m_{PANI}:m_{CNns} = 1:1) was used, the degradation efficiency of MB reached 98% within 40 min under simulated sunlight irradiation.

Hosseini et al. synthesized a ternary nanocomposite with *in-situ* oxidative polymerization, camphor sulfonic acid doped PANI-WO_3-multiwall carbon nanotube (CSA PANI-WO_3-CNT) [49]. The degradation rate of MB dye in 60 min illumination using this nanocomposite reached 91.40%, higher than that of free WO_3 (43.45%), free CSA PANI (48.4%), and CSA PANI-WO_3 binary nanocomposite (85.15%). A schematic illustration of MB photodegradation by CSA PANI-WO_3-CNT is shown in Fig. 3. During light irradiation, the electrons of CSA PANI and WO_3 were simultaneously excited. The transfer of electrons from the LUMO of CSA PANI (– 1.63 V vs. NHE) to the CB of WO_3 (0.6 V vs. NHE) and the holes from the VB of WO_3 (3.58 V vs. NHE) to the HOMO of CSA PANI (0.8 V vs. NHE) occurred for the appropriate band alignment between the inorganic semiconductor WO_3 and the polymeric semiconductor

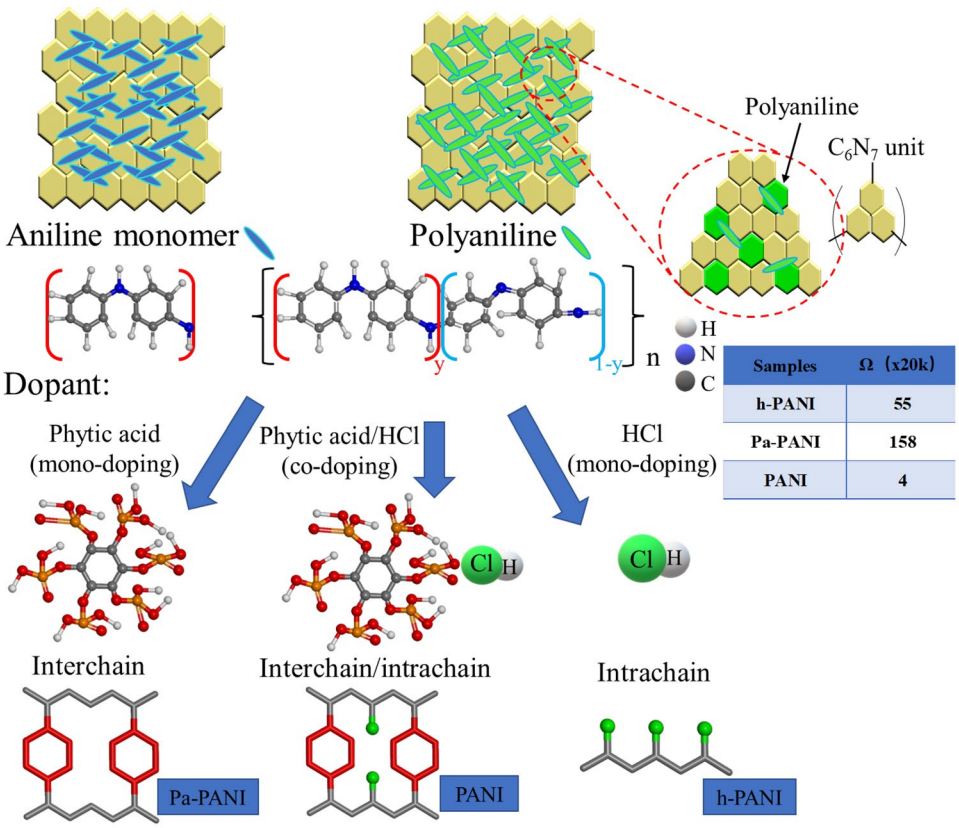

Fig. 2 Schematic displaying the preparation of PANI/CNns and the doping behavior of PA and HCl with interchain, intrachain, and interchain/intrachain doping on PANI

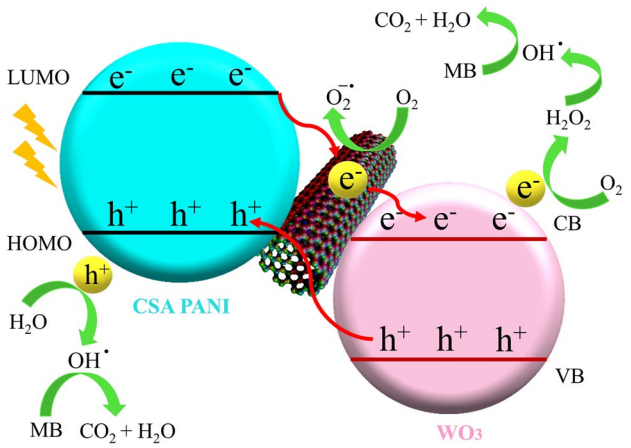

Fig. 3 Schematic presentation of photocatalytic mechanism for MB degradation in the presence of CSA PANI-WO3-CNT

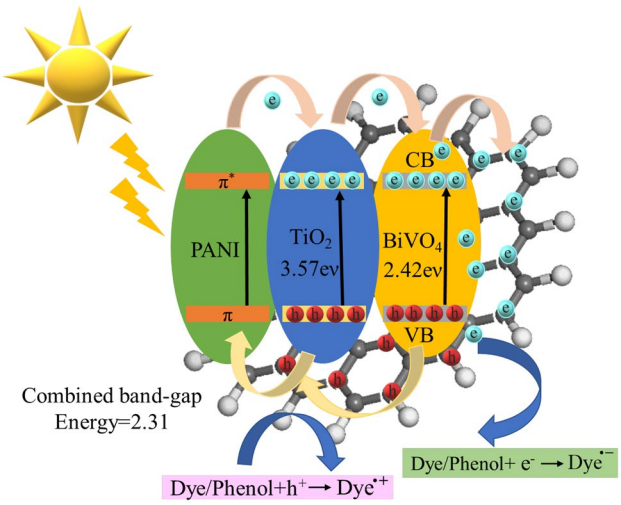

Fig. 4 Schematic diagram of dye/phenol degradation process

CSA PANI. Therefore, the electron–hole recombination was hindered. The transferred holes on the HOMO of CSA PANI reacted with H_2O to form hydroxyl radicals ($OH^•$), whereas the electrons in the CB of WO_3 reacted with oxygen molecules and H^+, producing H_2O_2 to further providing $OH^•$ radicals. Finally, the $OH^•$ radicals reacted in turn with MB molecules to produce CO_2 and H_2O. The CB of WO_3 was not conducive to the standard redox potential of $O_2/O_2^{•-}$ (− 0.046 V vs. NHE); therefore, superoxide anions ($O_2^{•-}$) cannot be obtained. The decomposition percentage of MB further increased in the presence of COOH-MWCNT, which could be the results of more negative energy position of CNT (− 0.1 V vs. NHE) than the standard redox potential of $O_2/O_2^{•-}$ and more $OH^•$ radicals were generated.

Zhao et al. prepared a novel nontoxic $BiVO_4$-GO-TiO_2-PANI (BVGT-PANI) composite with excellent photocatalytic performance in a one-pot hydrothermal reaction [50]. Under visible-light irradiation, PANI-modified BVGTA showed stronger photocatalytic activity for the degradation of MB than BVG ($BiVO_4$-GO) and BVGT ($BiVO_4$-GO-TiO_2), indicating a synergistic effect in the hybrid materials of polymer chain, GO flakes, and metal oxides. BVGTA showed the highest k_{app} rate constant of about 1.06×10^{-2} min^{-1}, which was 1.63 times faster than BVG and 2.94 times faster than BVGT. In addition, in vitro toxicity tests against *Bacillus subtilis* and *Staphylococcus aureus* showed that the nanometer photocatalyst was nontoxic. A schematic diagram of dye/phenol degradation using BVGT-PANI is shown in Fig. 4.

PANI can be combined with semiconductor nanomaterials such as titanium oxide, bismuth-based nanomaterials, ZnO, NiO, WO_3, and SnO_2 to prepare binary composite photocatalysts. Besides semiconductors, carbon-based materials such as carbon nanotubes (CNTs), graphene oxide (GO), and graphitic carbon nitride (g-C_3N_4) are suitable options for the hybridization of PANI. To achieve better photocatalysis, metal-oxide NPs, carbon-based materials, and other polymers together with PANI have been used to synthesize ternary or quaternary organo-inorganic photocatalytic nanocomposite materials to degrade MB under visible or UV light. The recently developed PANI-based materials as well as the photocatalytic testing conditions, and photodegradation efficiency for MB are shown in Table 1.

Degradation of RHB using PANI composites

RhB ($C_{28}H_{31}ClN_2O_3$) is widely used as a model molecule in the photodegradation of cationic xanthene class dye.

Steplin Paul Selvin et al. prepared zinc oxide activated charcoal PANI (ZACP) nanocomposite using a simple precipitation method [77]. The as-synthesized photocatalyst exhibited more photocatalytic activity than free ZnO on the degradation of RhB under visible-light irradiation, as the results of photosensitization and electron–hole pair separation by PANI in the composites were obtained. Also, the minimum loss of activity in recycling three times suggested good stability of the composite materials. Moreover, the mineralization of RhB was confirmed by evaluating chemicals and toxicity. A possible reaction mechanism of photocatalytic degradation of RhB in the presence of ZACP under visible-light irradiation is shown in Fig. 5. Compared with the CB and VB positions of ZnO, the LUMO and HOMO levels of PANI are higher. Under visible-light irradiation, PANI transfers excited electrons from the π orbital to the π^* orbital. These excited electrons are transferred from the LUMO of PANI to the CB of ZnO and react with water and oxygen to form hydroxyl and superoxide radicals. These hydroxyl and superoxide radicals react with the dye to form less toxic substances. Therefore, the addition of PANI can effectively separate rapid photogenerated

Table 1 Photocatalytic decomposition of MB on polyaniline composites

Photocatalyst	Irradiation Source	Total Irradiation Time (min)	Optimal Degradation Efficiency (%)	Optimal Rate Constant (min^{-1})	References (Year)
Biotemplate-SnO_2-PANI	Visible	210	91.36		[28] (2016)
PANi-NiO	Visible	300	76	0.005	[31] (2019)
GO/PANI/TiO_2	UV	60	98.9		[34] (2020)
PAni-TiO_2	UV	75	100		[40] (2020)
PANI-TiO_2	UV	90	86.35	0.022	[46] (2020)
PANI/$SrSnO_3$	UV	240	83	0.008	[47] (2019)
PANI/g-C_3N_4	Visible	40	98		[48] (2019)
CSA PANI-WO_3-CNT	Visible	60	91.40	0.044	[49] (2020)
$BiVO_4$-GO-TiO_2-PANI	Visible	180	85	0.001	[50] (2019)
PANI/MS-TiO_2	Visible	150	99.5	0.017	[51] (2016)
carbonized PANI/TiO_2	UV	60	100	0.078	[52] (2017)
$BiPO_4$-PANI	UV	120	95.8		[53] (2018)
	Visible	480	87.3		
Pani/Fe-TiO_2	UV	150	23	0.003	[54] (2019)
$BaZn_{0.2}Co_{0.2}Sn_{0.4}Fe_{11.2}O_{19}$/PANI	Visible	60	80	0.030	[55] (2019)
Pani/SiC-Fe	UV	300	22	0.001	[56] (2019)
Fe_2O_3@PANI-o-PDA	Visible	7200	95	0.001	[57] (2019)
$MoSe_2$-PANI	Visible	120	65		[58] (2019)
Co_2TiO_4/ $CoTiO_3$/Polyaniline	Visible	120	94.5		[59] (2019)
PANI-capped ZnO	UV	180	74	0.007	[60] (2020)
Fe_3O_4@TiO_2-PANI-Ag	Visible	90	100	0.004	[61] (2020)
$BiVO_4$/GO/PANI	Visible	180	73	0.001	[62] (2020)
PANI/ZnO	Visible	80	99.99	0.140	[63] (2020)
PANI/WO_3	Visible	120	84		[64] (2020)
PANI/$BiVO_4$/cellulose aerogel	Visible	60	99.72		[65] (2020)
g-C_3N_4-PANI-PPy	Visible	50	95.5	0.006	[66] (2021)
PANI/NiO	UV	30	100	0.168	[67] (2021)
	Visible	30	100	0.182	
Bi_2O_3/PANI	Visible	150	96.4	0.016	[68] (2021)
ZnO–MoS_2-PANI	Visible	60	99.6		[69] (2021)
PANI-rGO-ZnO	Visible	100	95	0.030	[70] (2021)
Bi_2O_3@PANI	UV	120	98.3		[71] (2021)
PANI-ZnO-Ho_2O_3-Sm_2O_3	Visible	60	94.7	0.047	[72] (2021)
Ag/PANI/$ZnTiO_3$	Visible	25	95.6		[73] (2021)
PANI	UV	30	92	0.118	[74] (2021)
NPANI			83	0.048	
PANI-ZnO	UV	150	95	0.071	[75] (2021)
PANI-Ag/ZnS	UV	60	94	0.651	[76] (2022)

electrons, thus improving the photocatalytic activity of ZACP nanocomposites.

In a pioneering work, Sayed et al. prepared CeO_2-PANI and ZrO_2-PANI composites in a solvent system of chloroform and 2-butanol [78]. The photocatalytic results showed that the degradation rate of RhB in 60 min of photolysis was 35 and 34% by CeO_2-PANI and ZrO_2-PANI, respectively. Photosensitization mechanism of PANI–ZrO_2/CeO_2 composite is shown in Fig. 6. The degradation products of RhB were quantitatively analyzed by LC–MS and GC–MS, and the specific degradation pathways were given. The degradation product at *m/z* of 415 is the deethyl product of RhB, probably due to the direct photolysis of RhB or the attack of •OH on RhB molecules. The degradation product with an *m/z* value of 387 can be attributed to the elimination of *N* substitutions in RhB molecule and the formation

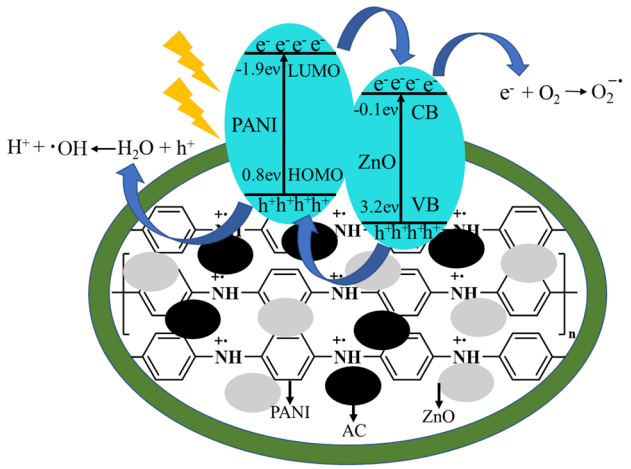

Fig. 5 Plausible photodegradation mechanism of RhB using ZACP under visible light irradiation

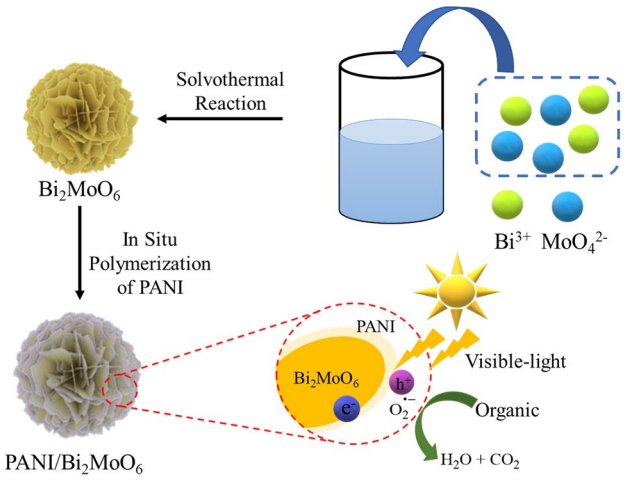

Fig. 7 Schematic diagram of the facile synthesis of PANI/Bi_2MoO_6 nanocomposites for the visible-light-driven photocatalytic degradation of organic pollutants

of *N*-deethyl degradation product. Then, it was replaced by •OH digestion to produce a degradation product with an *m/z* of 122. The degradation product with an *m/z* of 138 is formed mainly due to the two-step reaction between •OH and RhB molecules. The first step is hydrogen extraction reaction, and the second step is •OH addition reaction. A GC–MS analysis showed that the product with an *m/z* of 154 was the hydroxylation degradation product. The structure of RhB is further damaged by •OH, and a degradation product with an *m/z* of 132 is formed, also indicating that the synthetic material makes the molecular degradation of RhB close to mineralization.

Feng et al. reported the *in-situ* polymerization of PANI on the surface of Bi_2MoO_6 nanosheets to produce PANI/Bi_2MoO_6 nanocomposites, and the application for the visible-light-driven degradation of RhB [79]. As shown in Fig. 7, the molecular PANI layers covered the surface of flower-like Bi_2MoO_6 microspheres, which were composed of ultrathin nanosheets (13.8 ± 1.6 nm), and the intrinsic crystallinity of Bi_2MoO_6 was preserved in the polymerization of PANI. The optimized photodegradation rate for RhB reached up to ~ 100% in 120 min in the presence of $PANI_{0.5}$/Bi_2MoO_6. The degradation was consistent with a first-order kinetics with a high apparent rate constant of 0.0335 min^{-1} and acceptable recycling stability. Mechanism studies showed that both PANI and Bi_2MoO_6 in the nanocomposites can be excited to produce induced electrons and holes under visible-light irradiation. Bi_2MoO_6 ultrathin nanosheets covered with PANI molecules provided sufficient active sites for the aggregation of these electrons to capture oxygen molecules and produce superoxide radicals. Both the holes and superoxide radicals can degrade organic pollutants directly and played an important role in improving the photocatalytic performance.

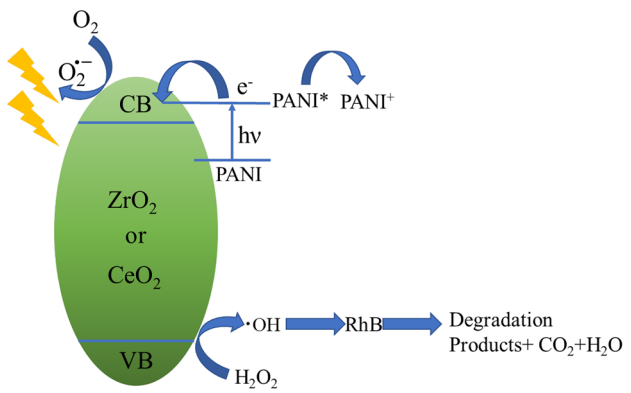

Fig. 6 Photosensitization mechanism of PANI–ZrO_2/CeO2 composite

Recently, Yu et al. studied the removal of organic pollutants such as RhB and phenol in high-salinity wastewater using Ag_3PO_4/PANI/Cr:$SrTiO_3$ ternary photocatalysts under visible-light irradiation [80]. Under the optimized conditions, the photocatalytic activities of Ag_3PO_4/PANI/Cr:$SrTiO_3$ composites on RhB and phenol reached 100% within 10 min and 18 min, respectively. The cyclability test showed that the ternary photocatalysts still maintained 92.25% catalytic activity after five cycles. With the increase in SO_4^{2-} concentration, the activity of Ag_3PO_4/PANI/Cr:$SrTiO_3$ to RhB remained at a high level, indicating that the catalyst had good tolerance of sulfate. Further analysis indicated the important contribution of photoinduced holes and superoxide radicals to the visible-light photocatalytic activity.

A variety of composite photocatalysts based on PANI doped with semiconductors, carbon-based materials, or

Table 2 Photocatalytic decomposition of RhB on polyaniline composites

Photocatalyst	Irradiation Source	Total Irradiation Time (min)	Optimal Degradation Efficiency (%)	Optimal Rate Constant (min^{-1})	References (Year)
PANI-Bi_2Se_3 NFs	Visible	25	97.7	0.147	[39] (2019)
Fe_3O_4/ZnO/BiOI/ PANI	Visible	180	99.2	0.023	[48] (2019)
PANI/MS-TiO_2	Visible	99.8	120	0.031	[51] (2016)
carbonized PANI/TiO_2	UV	90	96	0.033	[52] (2017)
PANI/$BiVO_4$/cellulose aerogel	Visible	60	98.24		[65] (2020)
PANI/NiO	UV	30	100	0.183	[67] (2021)
	Visible	30	100	0.198	
Zinc oxide activated charcoal polyaniline (ZACP)	Visible	120	95	0.031	[77] (2018)
ZrO_2-PANI	Visible	60	34	0.062	[78] (2018)
CeO_2-PANI			35	0.061	
PANI/Bi_2MoO_6	Visible	120	100	0.034	[79] (2019)
Ag_3PO_4/PANI/Cr:$SrTiO_3$	Visible	10	100	0.057	[80] (2020)
$MnFe_2O_4$/PANI	Visible	80	100	0.081	[81] (2016)
PANI/V_2O_5	Visible	300	79.5	0.005	[82] (2017)
PANI/grey-TiO_2	Visible	180	100		[83] (2017)
PANI/CeONP	UV	120	91	0.086	[84] (2018)
PANI/g-C_3N_4	Visible	150	42.7	0.014	[85] (2018)
BiOCl/PANI	Visible	25	99	0.153	[86] (2019)
Bi_5O_7I/PANI	Visible	60	84	0.031	[87] (2019)
M-PANI@AgI	Visible	180	99.64	0.030	[88] (2019)
PANI/Ag_3PO_4/$NiFe_2O_4$	Visible	40	100	0.133	[89] (2019)
Ta_3N_5@PANI	Visible	90	100	0.041	[90] (2019)
PANI/RGO	Visible	30	99.35	0.168	[91] (2019)
PANI–TiO_2	UV	120	91.8	0.021	[92] (2020)
$MoSe_2$-PANI	Visible	150	83.3	1.321	[93] (2020)
PANI-TiO_2/rGO	Visible	90	90.5	0.025	[94] (2020)
PANI-$CuFe_2O_4$	Visible	70	100	0.081	[95] (2020)
PANI-$YFeO_3$		110	100	0.048	
ZnS/CdS/PANI	Visible	135	96.5	0.017	[96] (2020)
PANI/GO/Cu_2O	Visible	150	68	0.007	[97] (2021)
rGH-PANI/BiOI	Visible	90	100	0.065	[98] (2021)
GH/PANI/Ag@AgCl	Visible	120	93.2		[99] (2021)
WO_3@PANI	Visible	120	90	0.018	[100] (2022)
Fe_3O_4@C/1D PANI/Ag@AgCl	Visible	14	95.9	0.226	[101] (2022)

other polymers were synthesized for the efficient removal of RhB in wastewater. As shown in Table 2, $MoSe_2$-PANI nanocomposite was synthesized and used as a photocatalyst for the removal of RhB dye [93]. The results indicated that the nanocomposite had the highest degradation rate constant of 1.3205 min^{-1} under visible-light irradiation when the weight ratio of $MoSe_2$ to PANI is 2:1.

Degradation of MO using PANI composites

MO ($C_{14}H_{14}N_3NaO_3S$), an anionic azo dye, remains in the environment for a long duration due to its low biodegradability. Thus, MO was always selected as a model dye to assess the photocatalytic ability of composite photocatalysts. Table 3 shows the compositions, photocatalytic testing

Table 3 Photocatalytic decomposition of MO on polyaniline composites

Photocatalyst	Irradiation Source	Total Irradiation Time (min)	Optimal Degradation Efficiency (%)	Optimal Rate Constant (min^{-1})	References (Year)
PANI-Bi_2Se_3 NFs	Visible	30	96.31	0.100	[39] (2019)
$MoSe_2$-PANI	Visible	150	94		[58] (2019)
Co_2TiO_4/$CoTiO_3$/Polyaniline	Visible	120	65.6		[59] (2019)
PANI/WO_3	Visible	120	86		[64] (2020)
PANI/Ag_3PO_4/$NiFe_2O_4$	Visible	25	94.97	0.154	[89] (2019)
Ag_2CO_3/Ag/PANI	Visible	60	71.9	0.018	[102] (2017)
$Co_{0.5}Mn_{0.5}Fe_2O_4$-PANI	Visible	120	92	0.023	[103] (2019)
TiO_2-DPA-PANI	UV	20	99.5	0.133	[104] (2019)
CF/RuO_2–TiO_2/DPA@PANI	Visible	45	100	0.083	[105] (2020)
PANI/ZnO	Visible	180	98.3	0.023	[106] (2016)
SiO_2-BiOCl@PANI@Pd	Visible	230	97	0.010	[107] (2017)
PANI-AlZnO	Visible	150	92.5	0.018	[108] (2017)
PANI/h-BN	UV	90	95		[109] (2018)
PANI/$MgIn_2S_4$	Visible	50	97	0.090	[110] (2019)
TiO_2/PANI	UV	120	90.9	0.016	[111] (2019)
	Visible	240	97.1	0.013	
PANI/SnS	Visible	40	81.4	0.040	[112] (2020)
CeO_2/PANI	Visible	240	45		[113] (2020)
BiOBr/BiOCl/PANI@TCPP	Visible	10	95		[114] (2020)
BiOBr/BiOCl/PANI@SnTCPP	Visible	10	96		
CPA/N-SWCNTS-GO-CE/CuO	UV	100	100		[115] (2021)
PANI-CdS/CeO_2/Ag_3PO_4	Visible	160	93.4	0.015	[116] (2021)
TiO_2/PANI-KpF	Visible	350	87.4	0.006	[117] (2021)

conditions, and photodegradation efficiency of PANI-based composite photocatalysts on MO degradation in recent years.

Chen et al. developed a facile two-step route to synthesize one-dimensional (1D) ternary Ag_2CO_3/Ag/PANI composite nanorods (CNRs) [102]. The structure of the as-prepared composite showed that Ag_2CO_3 nanorod cores coated with an intermediate layer of AgNPs and a sheath of conducting polymer PANI. By degrading MO under visible-light irradiation, the ternary photocatalyst showed enhanced photochemical current response and photocatalytic activity. The enhanced visible-light-driven photocatalytic activity can be attributed to the intermediate Ag between Ag_2CO_3 and PANI, which facilitates the separation efficiency of photogenerated carriers, and a Z-scheme charge transfer model was also proposed to understand the charge separation behaviors.

Jung et al. prepared $Co_{0.5}Mn_{0.5}Fe_2O_4$-PANI nanofibers through electrostatic spinning, heat treatment, and chemical polymerization, which had a 1D hollow heterostructure with a large surface area [103]. Irradiation of MO under visible-light irradiation showed that the photocatalytic degradation efficiency reached 92% within 120 min, and the kinetic constant was 115 times higher than that of the hollow $Co_{0.5}Mn_{0.5}Fe_2O_4$ nanofiber. In addition, the excellent magnetic properties of $Co_{0.5}Mn_{0.5}Fe_2O_4$-PANI nanofibers were confirmed by characterizing the spinel structure, which was conducive to the recovery of photocatalyst.

Mousli et al. reported a novel photocatalyst for the mineralization of organic dye pollutants modified with diazonium salts [104], and a TiO_2-DPA-PANI nanocomposite was prepared by *in-situ* oxidation after the diazonium pretreatment of TiO_2, which was used for the removal of MO under UV-light irradiation. As shown in Fig. 8, the material was synthesized in two pathways: preparation of PANI in an aqueous solution, and in the presence of pristine and diazonium-modified TiO_2. TiO_2-DPA-PANI nanocomposite exhibited excellent catalytic performance, and the degradation rate constant was 0.133 min^{-1}, much higher than 0.059 min^{-1} and 0.085 min^{-1} of free TiO_2 and TiO_2-PANI, respectively. Moreover, because the thick coating of PANI protected the following TiO_2, TiO_2-DPA-PANI could be recycled for five times without losing any photocatalytic activity. However, TiO_2-PANI can only be recycled for three times, and bare TiO_2 can be reused for one time.

Mousli et al. designed a series of related composites of cotton fabrics (CF) modified with mixed oxides to catalyze the degradation of MO under visible-light irradiation [105]. To be specific, the photocatalyst RuO_2-TiO_2 was coated on

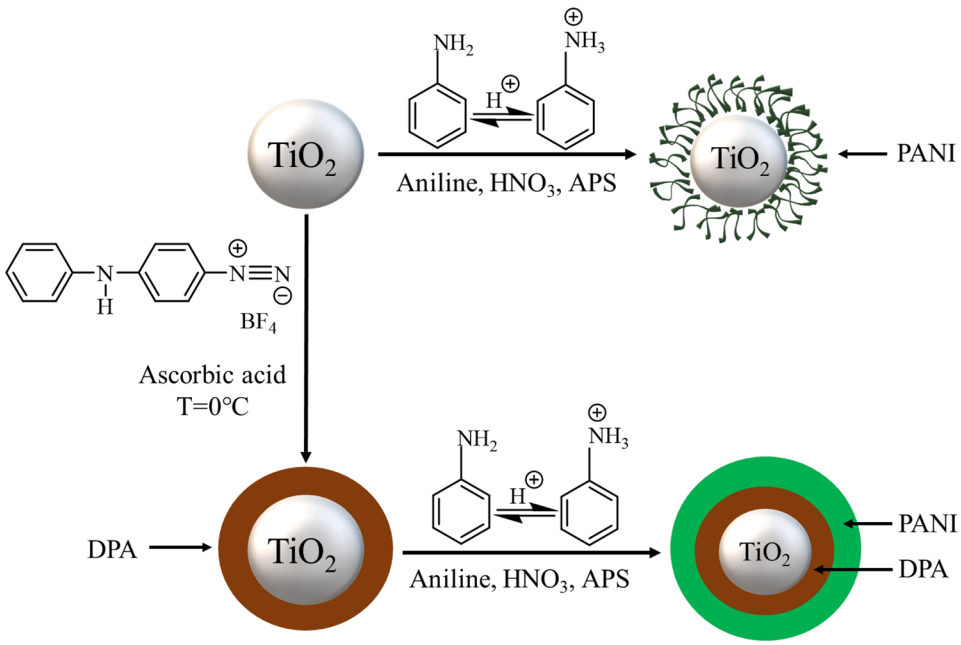

Fig. 8 General pathway for TiO_2-DPA-PANI and TiO_2-PANI nanocomposites

CF using dip-coating method. A layer of PANI was prepared by *in-situ* polymerization on 4-diphenylamine diazonium salt (DPA) modified RuO_2-TiO_2 NP coated CF. The CF/RuO_2-TiO_2/DPA@PANI hybrid photocatalyst exhibited better catalytic performance compared to other catalysts coated on CFs with a photodegradation rate constant of 0.0828 min^{-1}. Owing to the coupling action of the diphenyl amino group from diazonium salts, the PANI film was attached to the surface of RuO_2-TiO_2 and formed a strong O–N covalent bond with the fabric. The improvement in the catalytic performance was attributed to the strong interfacial interactions between the nanocomposite components and the synergistic effect of charge transfer between different interfaces of CF/RuO_2-TiO_2/DPA@PANI.

Photocatalytic decomposition of pharmaceuticals

From an environmental viewpoint, even the presence of a low concentration of pharmaceuticals in the wastewater effluent can be hazardous to aquatic organisms and human beings. However, the degradation of drugs is very difficult. The biological methods and physical precipitation methods such as centrifugation and flocculation are common techniques, but they have their own disadvantages [118]. In recent decades, the use of photocatalysts has attracted much attention in the photocatalytic degradation of organic pollutants because of its relatively low cost, environmentally friendly characteristic, sustainable treatment technology, and overcoming the shortcomings of conventional technologies [119]. The photodegradation efficiencies of PANI-based composite photocatalysts on different pharmaceuticals are summarized in Table 4.

PANI can also form a heterojunction photocatalyst with organic compounds in addition to inorganic semiconductor composite photocatalysts. Wang and Zhu et al. synthesized PANI/perylene diimide with a 3D structure (3D PANI/PDI) using an in-situ growth method, which was applied for the degradation of tetracycline (TC) under visible-light irradiation [120]. 20% PANI/PDI showed excellent catalytic performance and stability, mainly due to the following three aspects: (1) The incorporation of PANI skeleton enhanced the strength of PDI organic hydrogels, thereby increasing the stability of photocatalyst; (2) the 3D structure provided more active sites and electron transport channels; (3) the larger delocalized electron covalent structure and energy matching heterojunction structure formed between PANI and PDI improved the separation efficiency of photogenerated electrons. The proposed degradation mechanism included successive reaction with hydroxylation, dealkylation, aromatization, and ring-opening reactions of TC until complete mineralization under the attack of the main reactive species (H_2O_2 and h^+).

Design and synthesis of green materials capable of green photocatalysis is an important future research direction. Kumar et al. synthesized metal-free carbon-based photocatalysts in a simple way and showed high photocatalytic activity driven by visible light and solar light [121]. The catalysts are based on acidified g-C_3N_4 (ACN), PANI, reduced GO (RGO), and biochar to form a nanocomposite ACN/PANI/RGO@Biochar (APRB). Among them, biochar acted as an adsorbent, and RGO acted as an electronic medium. Thus, an efficient heterojunction could be

Table 4 Photocatalytic decomposition of pharmaceuticals on polyaniline composites

Pharmaceutical	Photocatalyst	Irradiation Source	Total Irradiation Time (min)	Optimal Degradation Efficiency (%)	Optimal Rate Constant (min^{-1})	References (Year)
Ciprofloxacin	PANI/ZrO_2	UV	120	96.6		[4] (2020)
Gemifloxacin mesylate	PANI/$SrSnO_3$	UV	240	100		[47] (2018)
Tetracycline	ZnO–MoS_2-PANI	Visible	60	94.5		[69] (2021)
Clavulanate potassium	PANI-rGO-ZnO	Visible	100	47	0.006	[70] (2021)
Ciprofloxacin	ZrO_2-PANI CeO_2-PANI	Visible	60	35 37		[78] (2018)
Propranolol Amitriptyline	TiO_2/polyaniline	UV	60	23 45		[119] (2018)
Tetracycline	PANI/PDI	Visible	120	70	0.009	[120] (2020)
Ibuprofen	ACN/PANI/RGO@Biochar	Visible	50	98.4	0.080	[121] (2019)
Ampicillin	ZnO/polyaniline	Visible	120	41		[122] (2012)
Sulfaquinoxaline	PANI/TiO_2	UV	90	100	0.060	[123] (2019)
Ciprofloxacin	Bi_2WO_6/PANI	Visible	90	98	0.041	[124] (2020)
Thiamphenicol	MIL-100(Fe)/PANI + H_2O_2	Visible	120	100	0.024	[125] (2020)
Ciprofloxacin	PAN@ZnONPs/MOF	Visible	70	97.2	0.050	[126] (2020)
Oxytetracycline	g-C_3N_4/PANI	Visible	100	86.2	0.064	[127] (2021)
Ciprofloxacin	rGO/Ag_3PO_4/PANI	Visible	15	86.2		[128] (2021)
Ciprofloxacin	CN-PANI-CQDs	Visible	90	87.6	0.114	[129] (2021)

produced with the appropriate position of CN, ACN, and PANI, and reduced the recombination of charge carriers to improve the photocatalytic activity. The experimental results show that the degradation rates of ibuprofen (IBN) and 2,4-dichlorophenoxyacetic acid (2,4-D) after 50 min irradiation under xenon lamp were 98.4% and 99.7%, respectively. The degradation pathway was analyzed by LCMS, and 40% and 42% of the total organic carbon was removed in 2 h for IBN and 2,4-D, respectively. Furthermore, the low toxicity of degradation products was determined by the cytotoxicity analysis of human peripheral blood cells.

Table 5 Photocatalytic decomposition of pesticides on polyaniline composites

Pesticide	Photocatalyst	Irradiation Source	Total Irradiation Time (min)	Optimal Degradation Efficiency (%)	Optimal Rate Constant (min^{-1})	References (Year)
Monocrotophos	Ag_3PO_4/polyaniline@g-C_3N_4	Visible	50	99.6		[5] (2020)
Diazinon	Co_2TiO_4/$CoTiO_3$/Polyaniline	Visible	120	98.3		[59] (2019)
Sulcotrione Clomazone	TiO_2/polyaniline	UV	60	94 32		[119] (2018)
Thiacloprid Clomazone Quinmerac Sulcotrione	TiO_2/polyaniline	Visible	240	13 28 27 35		[130] (2019)
Chlorpyrifos	CuO/TiO_2/PANI	Visible	90	95	0.032	[131] (2021)
Diuron	ZnR@CGR/PANI	Visible	40	100	0.009	[132] (2018)
Glyphosate	PANI/$ZnWO_4$/WO_3	Visible	60	98.4	0.071	[133] (2021)
2,4-Dichlorophenoxyacetic acid	PANI/TiO_2	UV	120	99.91	0.332	[134] (2022)
Triclopyr acid				90.72	0.217	

Photocatalytic decomposition of pesticides

Photocatalytic technology can also be used to deal with environmental pollution caused by the extensive use of pesticides in agriculture, and the recent progress is shown in Table 5.

Photocatalytic degradation of several types of pesticides was achieved using TiO_2 NPs modified with PANI (TP nanocomposites) [130]. After simulating solar radiation for 240 min, the degradation rates of thiacloprid, clomazone, quinmerac, and sulcotrione were 13%, 28%, 27%, and 35%, respectively. The cytotoxicity was less than 11% in all the cases, and the photocatalytic degradation efficiency was higher in distilled water than in environmental water. Moreover, pH was the main factor affecting the efficiency of sulcotrione removal. In addition, the addition of H_2O_2 as an electron acceptor decreased the degradation rate, whereas the addition of $KBrO_3$ increased the degradation rate.

A novel ternary CuO/TiO_2/PANI was used as a photocatalyst to degrade 95% of extremely toxic pesticide chlorpyrifos in water within 90 min illumination [131]. The nanocomposite was synthesized using a simple oxidation method and characterized by XRD, EDX, PL, and HR-TEM analyses.

Conclusion

This review shows that PANI is useful to improve the performance of composite photocatalysts for the photocatalytic degradation of hazardous chemicals including dyes, pharmaceuticals, and pesticides, focusing on the roles of PANI. The loading of PANI can substantially improve the photocatalytic activity by enhancing the separation of photogenerated carriers, expanding the light absorption range, increasing the adsorption of reactants, inhibiting photocorrosion, and reducing the formation of large aggregates. This review provides a systematic concept about how PANI can improve the performance of composite photocatalysts [9, 24, 45].

Acknowledgements This work was supported by Natural Science Foundation of Guizhou Province (NO. [2020]1Y028, [2020]1Y036), Research Project of Introduce Talents of Guizhou University (No. (2019)02), and National Natural Science Foundation of China (NO. 22161011).

References

1. Jumat NA, Khor SH, Basirun WJ et al (2021) Highly visible light active ternary polyaniline-TiO_2-Fe_3O_4 nanotube/nanorod for photodegradation of reactive black 5 dyes. J Inorg Organomet Polym Mater 31(5):2168–2181
2. Xu B, Wang X, Huang Y et al (2020) Electrospinning preparation of PAN/TiO_2/PANI hybrid fiber membrane with highly selective adsorption and photocatalytic regeneration properties. Chem Eng J 399:125749
3. Chhabra VA, Kaur R, Walia MS et al (2020) PANI/PbS QD nanocomposite structure for visible light driven photocatalytic degradation of rhodamine 6G. Environ Res 186:109615
4. Vijayalakshmi S, Kumar E, Venkatesh PS et al (2020) Preparation of zirconium oxide with polyaniline nanocatalyst for the decomposition of pharmaceutical industrial wastewater. Ionics 26(3):1507–1513
5. Balasubramanian J, Ponnaiah SK, Periakaruppan P et al (2020) Accelerated photodeterioration of class I toxic monocrotophos in the presence of one-pot constructed Ag_3PO_4/polyaniline@g-C_3N_4 nanocomposite: efficacy in light harvesting. Environ Sci Pollut Res 27(2):2328–2339
6. Namdarian A, Tabrizi GA, Arsalani N et al (2020) Synthesis of PANi nanoarrays anchored on 2D BiOCl nanoplates for photodegradation of Congo Red in visible light region. J Ind Eng Chem 81:228–236
7. Garrido-Cardenas JA, Esteban-García B, Agüera A et al (2020) Wastewater treatment by advanced oxidation process and their worldwide research trends. Int J Environ Res Public Health 17(1):170
8. Bhadra J, Parangusan H, Popelka A et al (2020) Electrospun Polystyrene/PANI-Ag fibers for organic dye removal and antibacterial application. J Environ Chem Eng 8(3):103746
9. Jangid NK, Jadoun S, Yadav A et al (2021) Polyaniline-TiO_2-based photocatalysts for dyes degradation. Polym Bull 78(8):4743–4777
10. McManamon C, Delaney P, Morris MA (2013) Photocatalytic properties of metal and non-metal doped novel sub 10 nm titanium dioxide nanoparticles on methyl orange. J Colloid Interface Sci 411:169–172
11. Abdelhaleem A, Chu W (2018) Monuron photodegradation using peroxymonosulfate activated by non-metal-doped TiO_2 under visible LED and the modeling via a parallel-serial kinetic approach. Chem Eng J 338:411–421
12. Zhang D, Gong J, Ma J et al (2013) A facile method for synthesis of N-doped ZnO mesoporous nanospheres and enhanced photocatalytic activity. Dalton Trans 42(47):16556–16561
13. Hossain SS, Tarek M, Munusamy TD et al (2020) Facile synthesis of CuO/CdS heterostructure photocatalyst for the effective degradation of dye under visible light. Environ Res 188:109803
14. Assis GC, Silva IMA, Dos Santos TV et al (2021) Photocatalytic properties of SnO_2/MoO_3 mixed oxides and their relation to the electronic properties and surface acidity. J Photoch Photobio A 407:113035
15. Soltan WB, Ammar S, Olivier C et al (2017) Influence of zinc doping on the photocatalytic activity of nanocrystalline SnO_2 particles synthesized by the polyol method for enhanced degradation of organic dyes. J Alloy Compd 729:638–647
16. Tie L, Yu C, Zhao Y et al (2018) Fabrication of WO_3 nanorods on reduced graphene oxide sheets with augmented visible light photocatalytic activity for efficient mineralization of dye. J Alloy Compd 769:83–91
17. Vahedi Gerdeh F, Feizbakhsh A, Konoz, E et al (2020) Copper sulphide-Zirconium dioxide nanocomposites photocatalyst with enhanced UV-light photocatalysis efficiency: structural and methodology. Int J Environ An Ch 1–15
18. Oliveros AN, Pimentel JAI, de Luna MDG et al (2021) Visible-light photocatalytic diclofenac removal by tunable vanadium pentoxide/boron-doped graphitic carbon nitride composite. Chem Eng J 403:126213
19. Rameshbabu R, Ravi P, Pecchi G et al (2021) Black Trumpet Mushroom-like ZnS incorporated with Cu_3P: Noble metal free photocatalyst for superior photocatalytic H_2 production. J Colloid Interf Sci 590:82–93
20. Ibrahim YO, Hezam A, Qahtan TF et al (2020) Laser-assisted synthesis of Z-scheme TiO_2/rGO/g-C_3N_4 nanocomposites for

highly enhanced photocatalytic hydrogen evolution. Appl Surf Sci 534:147578
21. Helmy ET, Abouellef EM, Soliman UA et al (2021) Novel green synthesis of S-doped TiO_2 nanoparticles using Malva parviflora plant extract and their photocatalytic, antimicrobial and antioxidant activities under sunlight illumination. Chemosphere 271:129524
22. Dong H, Zeng G, Tang L et al (2015) An overview on limitations of TiO_2-based particles for photocatalytic degradation of organic pollutants and the corresponding countermeasures. Water Res 79:128–146
23. Ambigadevi J, Senthil Kumar P, Vo DVN et al (2021) Recent developments in photocatalytic remediation of textile effluent using semiconductor based nanostructured catalyst: A review. J Environ Chem Eng 9(1):104881
24. Zhan C, Yu G, Lu Y et al (2017) Conductive polymer nanocomposites: a critical review of modern advanced devices. J Mater Chem C 5(7):1569–1585
25. Abukhadra MR, Shaban M, Sayed F et al (2018) Efficient photocatalytic removal of safarnin-O dye pollutants from water under sunlight using synthetic bentonite/polyaniline@Ni_2O_3 photocatalyst of enhanced properties. Environ Sci Pollut R 25(33):33264–33276
26. Cionti C, Della Pina C, Meroni D et al (2020) Photocatalytic and oxidative synthetic pathways for highly efficient PANI-TiO_2 nanocomposites as organic and inorganic pollutant sorbents. Nanomaterials 10(3):441
27. Zhang CL, Ma RH (2019) Synthesis and photocatalytic activity of MnV_{13}/GO/PANI composite catalysts. J Coord Chem 72(16):2735–2748
28. Karpuraranjith M, Thambidurai S (2016) Biotemplate-SnO_2 particles intercalated PANI matrix: Enhanced photo catalytic activity for degradation of MB and RY-15 dye. Polym Degrad Stabil 133:108–118
29. Abukhadra MR, Shaban M, Abd El Samad MA (2018) Enhanced photocatalytic removal of Safranin-T dye under sunlight within minute time intervals using heulandite/polyaniline@ nickel oxide composite as a novel photocatalyst. Ecotox Environ Safe 162:261–271. https://doi.org/10.1016/j.ecoenv.2018.06.081
30. Pant A, Tanwar R, Kaur B et al (2018) A magnetically recyclable photocatalyst with commendable dye degradation activity at ambient conditions. Sci Rep 8(1):14700
31. Vidya J, Balamurugan P (2019) Photocatalytic degradation of methylene blue using PANi-NiO nanocomposite under visible light irradiation. Mater Res Express 6(9):0950c8
32. Chatterjee MJ, Ahamed ST, Mitra M et al (2019) Visible-light influenced photocatalytic activity of polyaniline-bismuth selenide composites for the degradation of methyl orange, rhodamine B and malachite green dyes. Appl Surf Sci 470:472–483
33. Oh WC, Fatema KN, Liu Y et al (2020) Sonochemical synthesis of quaternary LaNiSbWO4-G-PANI polymer nanocomposite for photocatalytic degradation of Safranin-O and gallic acid under visible light irradiation. J Photoch Photobio A 394:112484
34. Baruah S, Kumar S, Nayak B et al (2021) Optoelectronically suitable graphene oxide-decorated titanium oxide/polyaniline hybrid nanocomposites and their enhanced photocatalytic activity with methylene blue and rhodamine B dye. Polym Bull 78(3):1703–1720
35. Abukhadra MR, Rabia M, Shaban M et al (2018) Heulandite/polyaniline hybrid composite for efficient removal of acidic dye from water; kinetic, equilibrium studies and statistical optimization. Adv Powder Technol 29(10):2501–2511
36. Gilja V, Vrban I, Mandić V et al (2018) Preparation of a PANI/ZnO composite for efficient photocatalytic degradation of acid blue. Polymers 10(9):940
37. BashirA HF, Yasmeen G et al (2019) Polyaniline based magnesium nanoferrite composites as efficient photocatalysts for the photodegradation of Indigo Carmine in aqueous solutions. Desalin Water Treat 164:368–377
38. Tang T, Li K, Dai L et al (2019) Visible-light driven conversion of pollutants into hydrogen and electricity based on a polyaniline dynamic electrode. J Electrochem Soc 166(6):F399–F405
39. El-Fawal EM, Younis SA, Moustafa YM et al (2020) Preparation of solar-enhanced AlZnO@carbon nano-substrates for remediation of textile wastewaters. J Environ Sci 92:52–68
40. Hasibur RK, Kumar KA (2020) Titanium-di-oxide (TiO_2) concentration-dependent optical and morphological properties of PAni-TiO_2 nanocomposite. Mat Sci Semicon Proc 105:104745
41. Gilja V, Živković I, Klaser T et al (2020) The impact of in situ polymerization conditions on the structures and properties of PANI/ZnO-based multiphase composite photocatalysts. Catalysts 10(4):400
42. Nair VR, Shetty Kodialbail V (2020) Floating bed reactor for visible light induced photocatalytic degradation of Acid Yellow 17 using polyaniline-TiO_2 nanocomposites immobilized on polystyrene cubes. Environ Sci Pollut Res 27(13):14441–14453
43. Zhang CL, Ma RH, Liu CT et al (2020) Preparation and photocatalytic performance of micro/nano structured β2-SiW11Mn doped polyaniline. J Coord Chem 73(20–22):3095–3108
44. Zhang CL, Ma RH, Liu CT et al (2020) Synthesis, characterization, and photocatalytic performance of a ternary composite catalyst α-SiW11Cr/PANI/ZnO. J Coord Chem 73(2):229–242
45. Stejskal J (2020) Interaction of conducting polymers, polyaniline and polypyrrole, with organic dyes: polymer morphology control, dye adsorption and photocatalytic decomposition. Chem Pap 74(1):1–54
46. Rahman KH, Kar AK (2020) Effect of band gap variation and sensitization process of polyaniline (PANI)-TiO_2 p-n heterojunction photocatalysts on the enhancement of photocatalytic degradation of toxic methylene blue with UV irradiation. J Environ Chem Eng 8(5):104181
47. Faisal M, Harraz FA, Ismail AA et al (2019) Novel synthesis of polyaniline/$SrSnO_3$ nanocomposites with enhanced photocatalytic activity. Ceram Int 45(16):20484–20492
48. Wu HH, Chang CW, Lu D et al (2019) Synergistic effect of hydrochloric acid and phytic acid doping on polyaniline-coupled g-C_3N_4 nanosheets for photocatalytic Cr(VI) reduction and dye degradation. ACS Appl Mater Inter 11(39):35702–35712
49. Hosseini MG, Sefidi PY, Mert AM et al (2020) Investigation of solar-induced photoelectrochemical water splitting and photocatalytic dye removal activities of camphor sulfonic acid doped polyaniline-WO_3-MWCNT ternary nanocomposite. J Mater Sci Technol 38:7–18
50. Zhao J, Biswas MRUD, Oh WC (2019) A novel $BiVO_4$-GO-TiO_2-PANI composite for upgraded photocatalytic performance under visible light and its non-toxicity. Environ Sci Pollut Res 26(12):11888–11904
51. Deng Y, Tang L, Zeng G et al (2016) Enhanced visible light photocatalytic performance of polyaniline modified mesoporous single crystal TiO_2 microsphere. Appl Surf Sci 387:882–893
52. Radoičić M, Ćirić-Marjanović G, Spasojević V et al (2017) Superior photocatalytic properties of carbonized PANI/TiO_2 nanocomposites. Appl Catal B-Environ 213:155–166
53. Yu WJ, Cheng Y, Zou T et al (2018) Preparation of $BiPO_4$-polyaniline hybrid and its enhanced photocatalytic performance. NANO 13(01):1850009
54. Koysuren O, Koysuren HN (2019) Photocatalytic activity of polyaniline/Fe-doped TiO_2 composites by in situ polymerization method. J Macromol Sci A 56(3):267–276
55. Mesdaghi S, Yousefi M, Hossaini sadr M et al (2019) The effect of PANI and MWCNT on magnetic and photocatalytic properties of substituted barium hexaferrite nanocomposites. Mater Chem Phys 236:121786
56. Koysuren O (2020) Improving ultraviolet light photocatalytic activity of polyaniline/silicon carbide composites by Fe-doping. J Appl Polym Sci 137(14):48524

57. Ossoss KM, Hassan MER, Al-Hussaini AS (2019) Novel Fe_2O_3@PANI-o-PDA core-shell nanocomposites for photocatalytic degradation of aromatic dyes. J Polym Res 26(8):199
58. Mittal H, Kumar A, Khanuja M (2019) In-situ oxidative polymerization of aniline on hydrothermally synthesized $MoSe_2$ for enhanced photocatalytic degradation of organic dyes. J Saudi Chem Soc 23(7):836–845
59. Rahimi-Nasrabadi M, Ghaderi A, Banafshe HR et al (2019) Preparation of Co_2TiO_4/$CoTiO_3$/Polyaniline ternary nanohybrids for enhanced destruction of agriculture poison and organic dyes under visible-light irradiation. J Mater Sci-Mater El 30(17):15854–15868
60. Chatterjee S, Kar AK (2020) Oxygen-vacancy-dependent photocatalysis for the degradation of MB dye using UV light and observation of Förster resonance energy transfer (FRET) in PANI-capped ZnO. J Phys Chem C 124(33):18284–18301
61. Al-saida B, Amer WA, Kandyel EE et al (2020) Enhanced dual catalytic activities of silver-polyaniline/titanium dioxide magnetic nanocomposite. J Photoch Photobio A 392:112423
62. Biswas MRUD, Ho BS, Oh WC (2020) Eco-friendly conductive polymer-based nanocomposites, $BiVO_4$/graphene oxide/polyaniline for excellent photocatalytic performance. Polym Bull 77(8):4381–4400
63. Sharma S, Kumar D, Khare N (2020) Hierarchical PANI/ZnO nanocomposite: synthesis and synergistic effect of shape-selective ZnO nanoflowers and polyaniline sensitization for efficient photocatalytic dye degradation and photoelectrochemical water splitting. Nanotechnology 31(46):465402
64. Szkoda M, Zarach Z, Trzciński K et al (2020) An aqueous exfoliation of WO_3 as a route for counterions fabrication-improved photocatalytic and capacitive properties of Polyaniline/WO_3 composite. Materials 13(24):5781
65. Wang L, Chen S, Wu P et al (2020) Enhanced optical absorption and pollutant adsorption for photocatalytic performance of three-dimensional porous cellulose aerogel with $BiVO_4$ and PANI. J Mater Res 35(10):1316–1328
66. Munusamy S, Sivaranjan K, Sabhapathy P et al (2021) Enhanced electrochemical and photocatalytic activity of g-C_3N_4-PANI-PPy nanohybrids. Synthetic Met 272:116669
67. Haspulat Taymaz B, Eskizeybek V, Kamış H (2021) A novel polyaniline/NiO nanocomposite as a UV and visible-light photocatalyst for complete degradation of the model dyes and the real textile wastewater. Environ Sci Pollut R 28(6):6700–6718
68. Li B, Li Y, Kang Y (2021) Simple hydrothermal preparation of novel Bi_2O_3/PANI heterojunction with significantly enhanced visible-light photocatalytic activity and stability. Mater Lett 286:129226
69. Sharma V, Maivizhikannan V, Rao VN et al (2021) Sea urchin shaped ZnO coupled with MoS2 and polyaniline as highly efficient photocatalysts for organic pollutant decomposition and hydrogen evolution. Ceram Int 47(7, Part B):10301–10313
70. Girija Shankar E, Aishwarya M, Khan A et al (2021) Efficient solar light photocatalytic degradation of commercial pharmaceutical drug and dye using rGO-PANI assisted c-ZnO heterojunction nanocomposites. Ceram Int 47(17):23770–23780
71. Dou W, Hu X, Kong L et al (2021) Photo-induced dissolution of Bi_2O_3 during photocatalysis reactions: Mechanisms and inhibition method. J Hazard Mater 412:125267
72. Mukhtar F, Munawar T, Nadeem MS et al (2021) Enhancement in carrier separation of ZnO-Ho_2O_3-Sm_2O_3 hetrostuctured nanocomposite with rGO and PANI supported direct dual Z-scheme for antimicrobial inactivation and sunlight driven photocatalysis. Adv Powder Technol 32(10):3770–3787
73. Faisal M, Jalalah M, Harraz FA et al (2021) A novel Ag/PANI/$ZnTiO_3$ ternary nanocomposite as a highly efficient visible-light-driven photocatalyst. Sep Purif Technol 256:117847
74. Haspulat Taymaz B, Taş R, Kamış H et al (2021) Photocatalytic activity of polyaniline and neutral polyaniline for degradation of methylene blue and malachite green dyes under UV light. Polym Bull 78(5):2849–2865
75. Turkten N, Karatas Y, Bekbolet M (2021) Preparation of PANI modified ZnO composites via different methods: structural, morphological and photocatalytic properties. Water 13(8):1025
76. Mazhar S, Qazi UY, Nadeem N et al (2022) Photocatalytic degradation of methylene blue using polyaniline-based silver-doped zinc sulfide (PANI-Ag/ZnS) composites. Environ Sci Pollut R 29(6):9203–9217
77. Steplin Paul Selvin S, Ganesh Kumar A, Sarala L et al (2018) Photocatalytic degradation of rhodamine B using zinc oxide activated charcoal polyaniline nanocomposite and its survival assessment using aquatic animal model. ACS Sustain Chem Eng 6(1):258–267
78. Shah AHA, Akhlaq S, Sayed M et al (2018) Synthesis and characterization of polyaniline-zirconium dioxide and polyaniline-cerium dioxide composites with enhanced photocatalytic degradation of rhodamine B dye. Chem Pap 72(10):2523–2538
79. Feng T, Yin H, Jiang H et al (2019) Design and fabrication of polyaniline/Bi_2MoO_6 nanocomposites for enhanced visible-light-driven photocatalysis. New J Chem 43(24):9606–9613
80. Yu X, Lin Y, Liu H et al (2020) Photocatalytic performances of heterojunction catalysts of silver phosphate modified by PANI and Cr-doped $SrTiO_3$ for organic pollutant removal from high salinity wastewater. J Colloid Interf Sci 561:379–395
81. Zeng S, Yang J, Qiu X et al (2016) Magnetically recyclable $MnFe_2O_4$/polyaniline composite with enhanced visible light photocatalytic activity for rhodamine B degradation. J Ceram Soc Jpn 124(10):1152–1156
82. Kundu S, Satpati B, Kar T et al (2017) Microstructure characterization of hydrothermally synthesized PANI/$V_2O_5{\cdot}nH_2O$ heterojunction photocatalyst for visible light induced photodegradation of organic pollutants and non-absorbing colorless molecules. J Hazard Mater 339:161–173
83. Xu S, Han Y, Xu Y et al (2017) Fabrication of polyaniline sensitized grey-TiO_2 nanocomposites and enhanced photocatalytic activity. Sep Purif Technol 184:248–256
84. Samai B, Bhattacharya SC (2018) Conducting polymer supported cerium oxide nanoparticle: Enhanced photocatalytic activity for waste water treatment. Mater Chem Phys 220:171–181
85. Zhou T, Fu S, Ma L et al (2018) Conjugated system in metal-free 1D polyaniline nanotubes/carbon nitride hollow composites with strong adsorption and enhanced visible-light photocatalytic activities. J Mater Sci-Mater El 29(5):4266–4275
86. Tang Y, Zhou P, Wang K et al (2019) BiOCl/ultrathin polyaniline core/shell nanosheets with a sensitization mechanism for efficient visible-light-driven photocatalysis. Sci China Mater 62(1):95–102
87. Wang L, Li X, Tang ZC et al (2019) Preparation and photocatalytic performance of Bi_5O_7I/PANI composites. Chinese J Inorg Chem 35(2):271–276
88. Liu X, Zhu H, Wu J et al (2019) The improved photocatalytic capacity derived from AgI-modified mesoporous PANI spherical shell with open pores. Res Chem Intermediat 45(5):2587–2603
89. Chen Y, Zhu P, Duan M et al (2019) Fabrication of a magnetically separable and dual Z-scheme PANI/Ag_3PO_4/$NiFe_2O_4$ composite with enhanced visible-light photocatalytic activity for organic pollutant elimination. Appl Surf Sci 486:198–211
90. Niu B, Xu Z (2019) A stable Ta_3N_5@PANI core-shell photocatalyst: Shell thickness effect, high-efficient photocatalytic performance and enhanced mechanism. J Catal 371:175–184
91. Mitra M, Ahamed ST, Ghosh A et al (2019) Polyaniline/reduced graphene oxide composite-enhanced visible-light-driven

photocatalytic activity for the degradation of organic dyes. ACS Omega 4(1):1623–1635
92. Majumdar S, Mahanta D (2020) Deposition of an ultra-thin polyaniline coating on a TiO_2 surface by vapor phase polymerization for electrochemical glucose sensing and photocatalytic degradation. RSC Adv 10(30):17387–17395
93. Mittal H, Khanuja M (2020) Optimization of $MoSe_2$ nanostructure by surface modification using conducting polymer for degradation of cationic and anionic dye: Photocatalysis mechanism, reaction kinetics and intermediate product study. Dyes Pigm 175:108109
94. Ma J, Dai J, Duan Y et al (2019) Fabrication of PANI-TiO_2/rGO hybrid composites for enhanced photocatalysis of pollutant removal and hydrogen production. Renew Energ 156:1008–1018
95. Mo Q, Zeng S, Yang J et al (2020) Polyaniline-ferrite nanocomposite as a new magnetically recyclable photocatalyst with enhanced photocatalytic activity. J Ceram Soc Jpn 128(3):135–141
96. Ali H, Mansor ES (2020) Co-sensitization of mesoporous ZnS with CdS and polyaniline for efficient photocatalytic degradation of anionic and cationic dyes. Colloid Interfac Sci 39:100330
97. Zhang D, Yang J, Qiao G et al (2021) Facile two-step synthesis of nanofiber polyaniline/graphene/cuprous oxide composite with enhanced photocatalytic performance. Appl Nanosci 11(3):983–993
98. Wang X, Zhu J, Yu X et al (2021) Enhanced removal of organic pollutant by separable and recyclable rGH-PANI/BiOI photocatalyst via the synergism of adsorption and photocatalytic degradation under visible light. J Mater Sci Technol 77:19–27
99. Chen F, Liang W, Qin X et al (2021) Ag@AgCl photocatalyst loaded on the 3D graphene/PANI hydrogel for the enhanced adsorption-photocatalytic degradation and in situ SERS monitoring properties. ChemistrySelect 6(17):4166–4177
100. Naciri Y, Hsini A, Bouziani A et al (2022) Z-scheme WO_3/PANI heterojunctions with enhanced photocatalytic activity under visible light: A depth experimental and DFT studies. Chemosphere 292:133468
101. Chen Q, Liang W, Shi X et al (2022) Photodegradation and in-Situ SERS Monitoring Properties of Ag@AgCl Anchored on Sea Urchin-shaped Fe_3O_4@C/1D PANI Nanoparticles. ChemistrySelect 7(9):e202104495
102. Chen F, Wu Y, Ning J et al (2017) Facile preparation of ternary Ag_2CO_3/Ag/PANI composite nanorods with enhanced photoactivity and stability. J Mater Sci 52(8):4521–4531
103. Jung HR, Kim KN, Lee WJ (2019) Heterostructured Co0.5Mn0.5Fe2O4-polyaniline nanofibers: highly efficient photocatalysis for photodegradation of methyl orange. Korean J Chem Eng 36(5):807–815
104. Mousli F, Chaouchi A, Hocine S et al (2019) Diazonium-modified TiO_2/polyaniline core/shell nanoparticles. Structural characterization, interfacial aspects and photocatalytic performances. Appl Surf Sci 465:1078–1095
105. Mousli F, Khalil AM, Maurel F et al (2020) Mixed oxide-polyaniline composite-coated woven cotton fabrics for the visible light catalyzed degradation of hazardous organic pollutants. Cellulose 27(13):7823–7846
106. Saravanan R, Sacari E, Gracia F et al (2016) Conducting PANI stimulated ZnO system for visible light photocatalytic degradation of coloured dyes. J Mol Liq 221:1029–1033
107. Tian Y, Li W, Zhao C et al (2017) Fabrication of hollow mesoporous SiO_2-BiOCl@PANI@Pd photocatalysts to improve the photocatalytic performance under visible light. Appl Catal B-Environ 213:136–146
108. Mitra M, Ghosh A, Mondal A et al (2017) Facile synthesis of aluminium doped zinc oxide-polyaniline hybrids for photoluminescence and enhanced visible-light assisted photo-degradation of organic contaminants. Appl Surf Sci 402:418–428
109. Shahabuddin S, Khanam R, Khalid M et al (2018) Synthesis of 2D boron nitride doped polyaniline hybrid nanocomposites for photocatalytic degradation of carcinogenic dyes from aqueous solution. Arab J Chem 11(6):1000–1016
110. Jing L, Xu Y, Xie M et al (2019) Three dimensional polyaniline/$MgIn_2S_4$ nanoflower photocatalysts accelerated interfacial charge transfer for the photoreduction of Cr(VI), photodegradation of organic pollution and photocatalytic H_2 production. Chem Eng J 360:1601–1612
111. Sun X, Sun B, Gong Q et al (2019) Double-shell structural polyaniline-derived TiO2 hollow spheres for enhanced photocatalytic activity. Transit Metal Chem 44(6):555–564
112. Yao K, Liu Y, Yang H et al (2020) Polyaniline-modified 3D-spongy SnS composites for the enhanced visible-light photocatalytic degradation of methyl orange. Colloid Surface A 603:125240
113. Li YS, Fang A, Lee GJ et al (2020) Preparation and photocatalytic properties of heterostructured ceria/polyaniline nanoparticles. Catalysts 10:732
114. Yaghoubi-berijani M, Bahramian B (2020) Synthesis, and new design into enhanced photocatalytic activity of porphyrin immobilization on the surface of bismuth oxyhalides modifed with polyaniline. J Inorg Organomet Polym Mater 30(11):4637–4654
115. Katowah DF, Saleh SM, Alqarni SA et al (2021) Network structure-based decorated CPA@CuO hybrid nanocomposite for methyl orange environmental remediation. Sci Rep 11(1):5056
116. Taddesse AM, Bekele T, Diaz I et al (2021) Polyaniline supported CdS/CeO_2/Ag_3PO_4 nanocomposite: An "A-B" type tandem n-n heterojunctions with enhanced photocatalytic activity. J Photoch Photobio A 406:113005
117. Gapusan RB, Balela MDL (2022) Visible light-induced photocatalytic and antibacterial activity of TiO_2/polyaniline-kapok fber nanocomposite. Polym Bull 79:3891–3910
118. Wang H, Zhang G, Gao Y (2010) Photocatalytic degradation of metronidazole in aqueous solution by niobate $K_6Nb_{10.8}O_{30}$. Wuhan Univ J Nat Sci 15(4):345–349
119. Šojić Merkulov DV, Despotović VN, Banić ND et al (2018) Photocatalytic decomposition of selected biologically active compounds in environmental waters using TiO_2/polyaniline nanocomposites: Kinetics, toxicity and intermediates assessment. Environ Poll 239:457–465
120. Dai W, Jiang L, Wang J et al (2020) Efficient and stable photocatalytic degradation of tetracycline wastewater by 3D Polyaniline/Perylene diimide organic heterojunction under visible light irradiation. Chem Eng J 397:125476
121. Kumar A, Sharma G, Naushad M et al (2019) Visible photodegradation of ibuprofen and 2,4-D in simulated waste water using sustainable metal free-hybrids based on carbon nitride and biochar. J Environ Manage 231:1164–1175
122. Nosrati R, Olad A, Maramifar R (2012) Degradation of ampicillin antibiotic in aqueous solution by ZnO/polyaniline nanocomposite as photocatalyst under sunlight irradiation. Environ Sci Pollut R 19(6):2291–2299
123. Sandikly N, Kassir M, El Jamal M et al (2021) Comparison of the toxicity of waters containing initially sulfaquinoxaline after photocatalytic treatment by TiO_2 and polyaniline/TiO_2. Environ Technol 42(3):419–428
124. Tahir MB, Nawaz T, Nabi G et al (2020) Photocatalytic degradation and hydrogen evolution using bismuth tungstate based nanocomposites under visible light irradiation. Int J Hydrogen Energ 45(43):22833–22847
125. An J, Li Y, Chen W et al (2020) Electrochemically-deposited PANI on iron mesh-based metal-organic framework with enhanced visible-light response towards elimination of thiamphenicol and E. coli. Environ Res 191:110067

126. Shoueir K, Wassel AR, Ahmed MK et al (2020) Encapsulation of extremely stable polyaniline onto Bio-MOF: Photo-activated antimicrobial and depletion of ciprofloxacin from aqueous solutions. J Photoch Photobio A 400:112703
127. Yu C, Tan L, Shen S et al (2021) In situ preparation of g-C_3N_4/polyaniline hybrid composites with enhanced visible-light photocatalytic performance. J Environ Sci 104:317–325
128. Wang J, Yu X, Fu X et al (2021) Accelerating carrier separation of Ag_3PO_4 via synergetic effect of PANI and rGO for enhanced photocatalytic performance towards ciprofloxacin. Mat Sci Semicon Proc 121:105329
129. Balakumar V, Ramalingam M, Sekar K et al (2021) Fabrication and characterization of carbon quantum dots decorated hollow porous graphitic carbon nitride through polyaniline for photocatalysis. Chem Eng J 426:131739
130. Lazarević MJ, Despotović VN, Šojić Merkulov DV et al (2019) Photodegradation of selected pesticides: Photocatalytic activity of bare and PANI-modified TiO_2 under simulated solar irradiation. J Serb Chem Soc 84(12):1455–1468
131. Nekooie R, Shamspur T, Mostafavi A (2019) Novel CuO/TiO_2/PANI nanocomposite: Preparation and photocatalytic investigation for chlorpyrifos degradation in water under visible light irradiation. J Photoch Photobio A 407:113038
132. Anirudhan TS, Shainy F, Manasa Mohan A (2018) Fabrication of zinc oxide nanorod incorporated carboxylic graphene/polyaniline composite and its photocatalytic activity for the effective degradation of diuron from aqueous solutions. Sol Energy 171:534–546
133. Barik B, Mishra M, Dash P (2021) Ionic liquid-assisted synthesis of a novel PANI/$ZnWO_4$/WO_3 ternary nanocomposite: a facile double electron transfer photocatalyst for efficient degradation of a herbicide. Environ Sci Nano 8(9):2676–2692
134. Moradeeya PG, Kumar MA, Sharma A et al (2022) Conductive polymer layered semiconductor for degradation of triclopyr acid and 2,4-dichlorophenoxyacetic acid from aqueous stream using coalesce adsorption-photocatalysis technique. Chemosphere 298:134360